

Supplementary Information

Molecular Series-Tunneling Junctions

Kung-Ching Liao,[†] Liang-Yan Hsu,^{#,‡} Carleen M. Bowers,^{#,†} Herschel Rabitz,^{*,‡} and

George M. Whitesides^{*,†,§,‡}

[†]Department of Chemistry and Chemical Biology, Harvard University,

12 Oxford Street, Cambridge, Massachusetts 02138 United States,

[‡]Department of Chemistry, Princeton University, Princeton, New Jersey 08544, United States,

[§]Wyss Institute for Biologically Inspired Engineering, Harvard University,

60 Oxford Street, Cambridge, Massachusetts 02138 United States, and

[‡]Kavli Institute for Bionano Science & Technology, Harvard University,

29 Oxford Street, Massachusetts 02138 United States

[#]Equal contributions

*Corresponding author, email:

hrabitz@princeton.edu (H.R.), gwhitesides@gmwgroup.harvard.edu (G.M.W.)

Contents:

1. Experiment Details
2. Figures S1 to S4 and Table S1
3. Summary of Transmission Theory and the derivations of eq. 2.
4. References

Experimental Details

Materials. All monolayer precursors—HO₂C(CH₂)_nH (**O₂C-C_n**; n = 4, 6, 8, 10), HO₂C(C₆H₄)_m(CH₂)_nH (**O₂C-Ph_mC_n**; m = 1, 2 and n = 2, 4, 6, 8), HO₂C(CH₂)_{2n}(C₆H₄)_mH (**O₂C-C_nPh_m**; m = 1, 2 and n = 2, 4, 6, 8), HO₂C(CH₂)₂(C₆H₄)(CH₂)₂H (**O₂C-C₂PhC₂**), and HO₂C(C₆H₄)-X-(C₆H₄)H (X = ethylene (–CH₂CH₂–; **O₂C-PhCH₂–CH₂Ph**), vinylene (–CH=CH–; **O₂C-PhCH=CHPh**), and acetylene (–C≡C–; **O₂C-PhC≡CPh**))—are commercially available (Alfa Aesar; Wako Chemicals; Oakwood Chemical; Santa Cruz Biotechnology; Sigma-Aldrich; TCI), and all carboxylic acids (% purities are equal or above 95%) were used as received. All organic solvents were analytical grade (99%, Sigma-Aldrich) and were used as supplied unless otherwise specified.

SAMs of Organic Carboxylates on Ag(/AgO_x) as Model Systems for Studying Tunneling.

Most studies of charge transport—using single-molecule or large-area junctions—commonly use SAMs of organic thiolates on Au or Ag.¹⁻⁴ Due to the limited number of readily available organic thiols/thiolates, and the difficulties of working with these compounds (which are oxygen-sensitive and highly nucleophilic), molecular systems based on the thiolate anchoring group have been largely restricted to simple molecular structures. Carboxylic acids were clearly identified by collective work of Allara, Nuzzo, and Tao as a class of molecules that formed stable, ordered SAMs on Ag.⁵⁻⁸ Since a very wide range of organic carboxylic acids are easily obtained (either commercially or through synthesis), and both these compounds and SAMs on silver are very stable to oxidation, they made excellent subjects for physical-organic studies of tunneling.

Preparation of SAMs. The preparation of SAMs of organic carboxylates on Ag follows published procedures:⁸⁻¹⁰ In brief, SAMs were formed by introducing freshly prepared template-stripped silver (Ag^{TS}) substrates¹¹ into a solution of the carboxylic acid (1 mM) in equal volume

mixture of anhydrous tetrahydrofuran (THF) and *n*-hexadecane for 5 minutes at ambient conditions. The resulting SAMs were washed three times with anhydrous THF (1 mL each time), and dried under a gentle stream of nitrogen.

Junction Measurements. We use “selected” unflattened conical EGaIn¹² to contact the surface of SAM-bound Ag^{TS}.^{11,13} In order to extract the current density (J , in A/cm²), the EGaIn contact area ($1500 \pm 150 \mu\text{m}^2$) was determined from the diameter of the contact region estimated by the optical microscopy.¹⁴⁻¹⁶ For each monolayer, at least 280 J – V curves were measured (three junctions made by a fresh EGaIn tip, 21 traces measured on a junction) from three different substrates.^{16,17} The $J(V)$ measurements were collected in a voltage scan mode between +0.5 and –0.5 V, back and forth (0 V \rightarrow +0.5 V; +0.5 V \rightarrow 0 V; 0 V \rightarrow –0.5 V; –0.5 V \rightarrow 0 V), in steps of 0.05 V with a 0.02 second delay between scans.^{13,15,17-19} We calculate the yield of working junctions by dividing the number of non-shortening junctions by the total number of measured junctions ($\times 100$).^{17,19} The junction measurements of **O₂C-C_n**, **O₂C-Ph_m**, **O₂C-C₂Ph**, and **O₂C-C₄Ph** were published elsewhere.^{10,20}

Figure S1. Log-current density ($\log|J|$) versus bias (V) for junctions of the form $\text{Ag}^{\text{TS}}\text{O}_2\text{C-Ph}_m\text{C}_n//\text{Ga}_2\text{O}_3/\text{EGaIn}$ ($m = 0, 1, 2$ and $n = 0, 2, 4, 6, 8, 10$) with increasing chain lengths. Rectification of current was not observed.

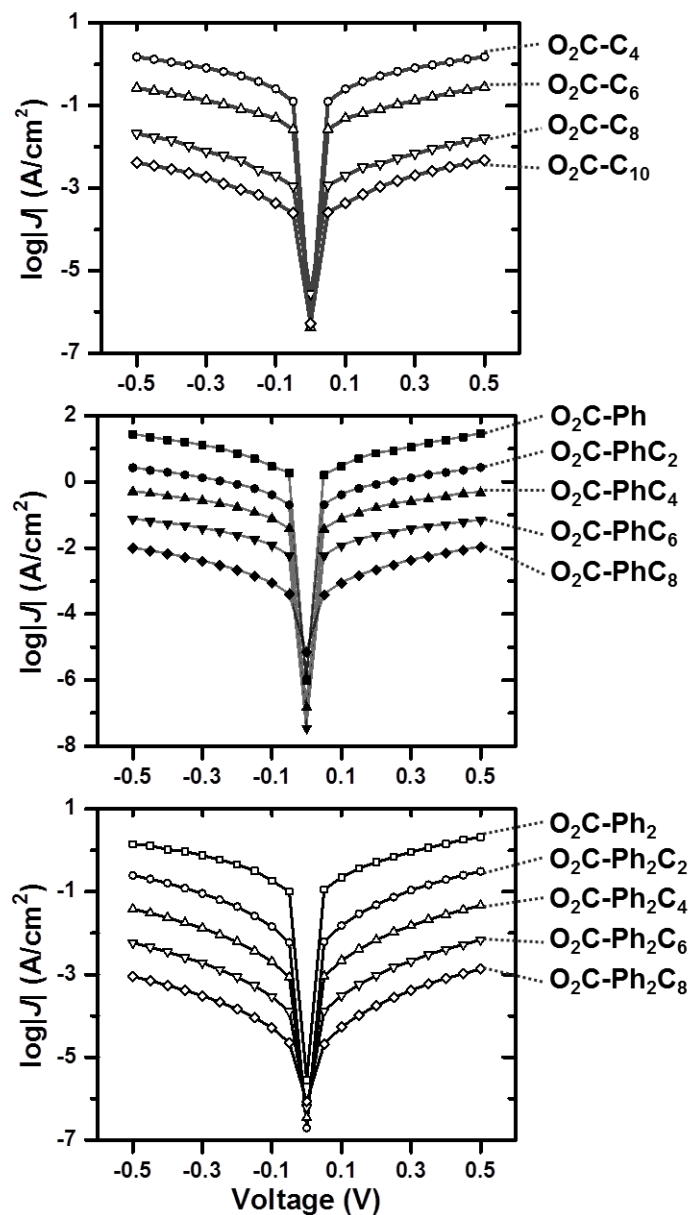


Figure S2. Log-current density ($\log|J|$) versus bias (V) for junctions of the form $\text{Ag}^{\text{TS}}\text{O}_2\text{C-C}_n\text{Ph}_m/\text{Ga}_2\text{O}_3/\text{EGaIn}$ ($m = 1, 2$ and $n = 0, 2, 4, 6, 8$) with increasing chain lengths. Rectification of current was not observed.

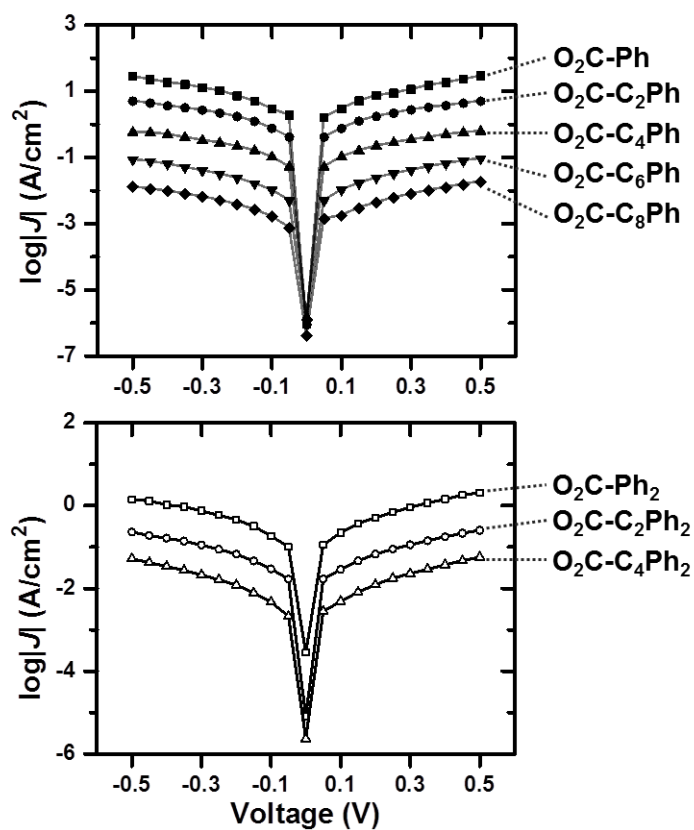


Figure S3. Histograms of $\log|J|$ data derived from (a) **O₂C-C_n**, (b) **O₂C-PhC_n**, and (c) **O₂C-Ph₂C_n** ($n = 2, 4, 6, 8, 10$) at -0.5 V. Each histogram is fitted with a Gaussian curve (black curve).

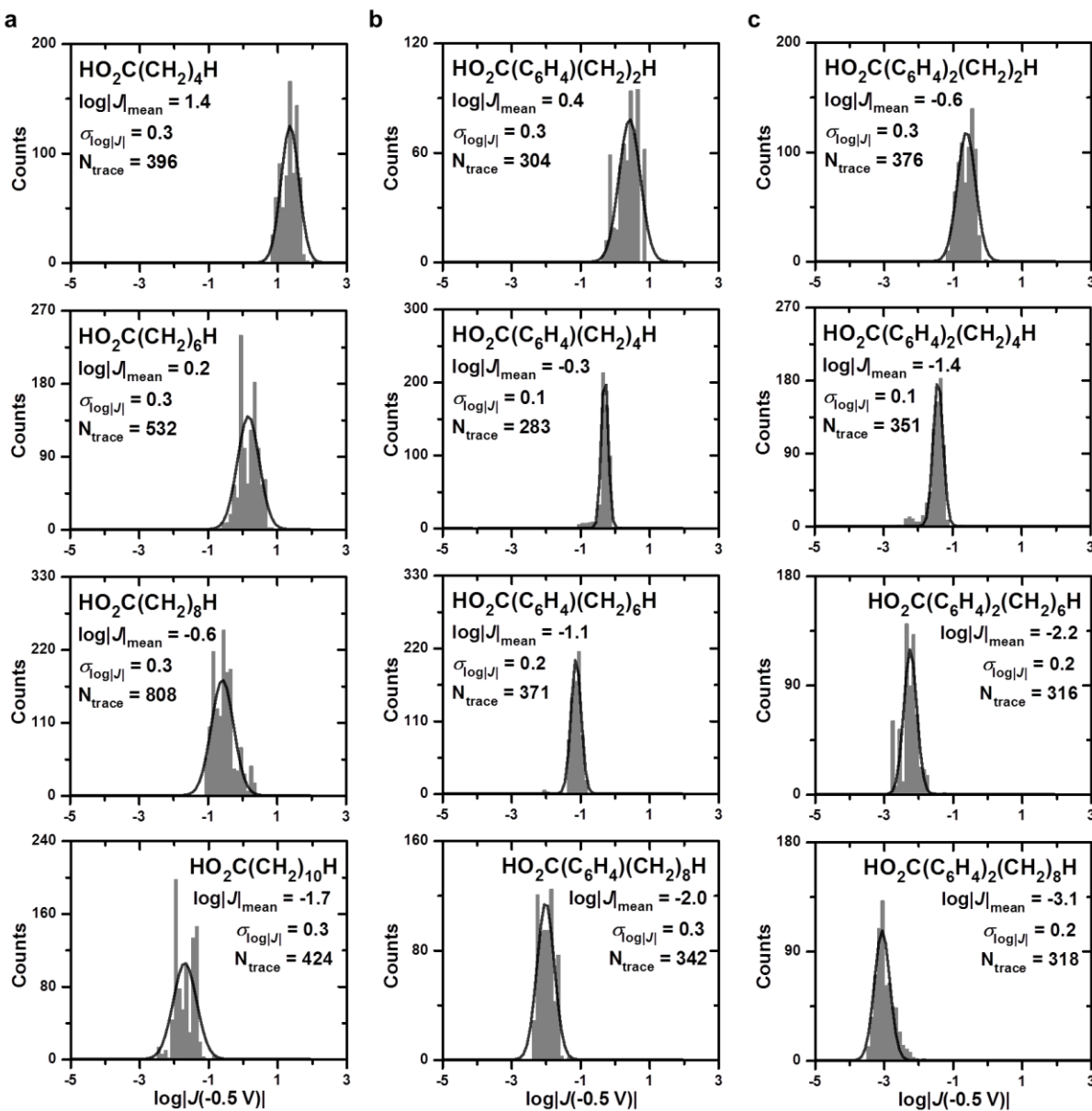


Figure S4. Histograms of $\log|J|$ data derived from (a) $\text{O}_2\text{C-C}_n\text{Ph}$, and (c) $\text{O}_2\text{C-C}_n\text{Ph}_2$ ($n = 2, 4, 6, 8$) at -0.5 V. Each histogram is fitted with a Gaussian curve (black curve).

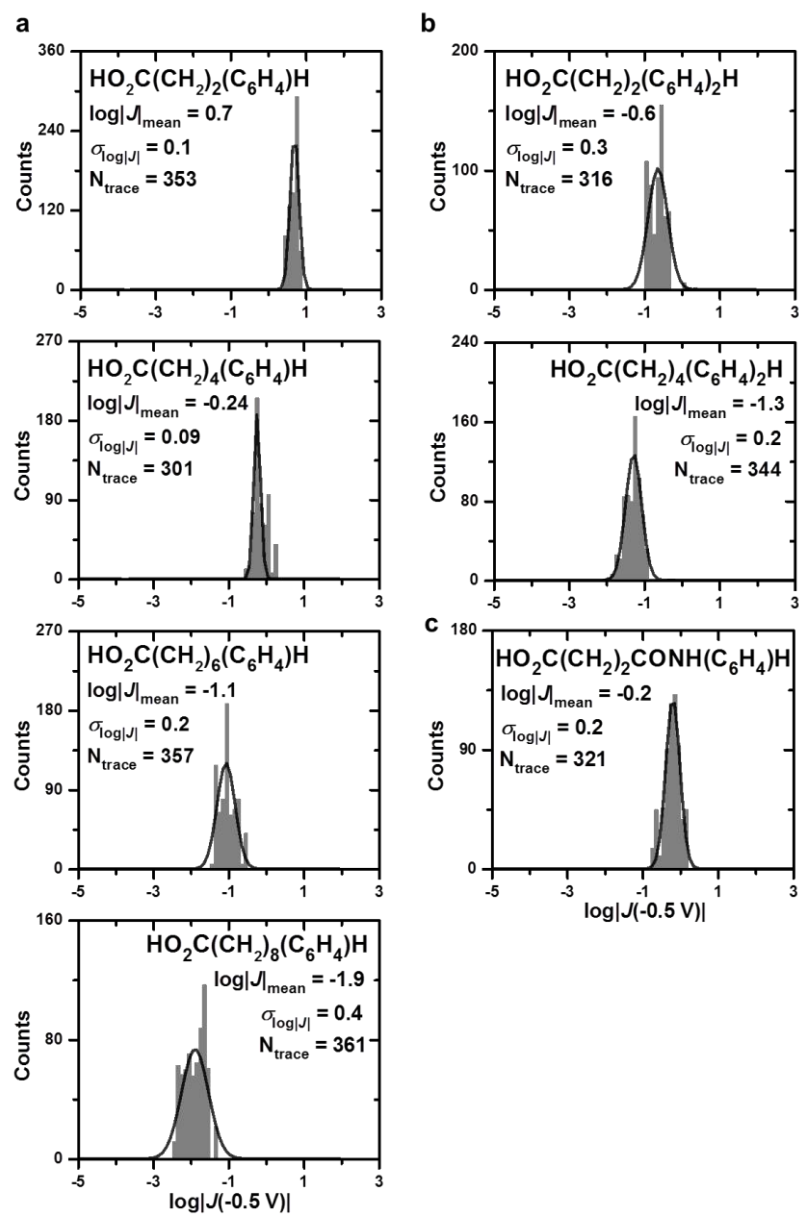
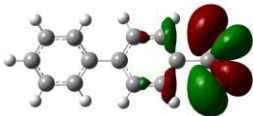
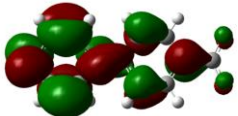
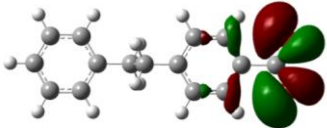
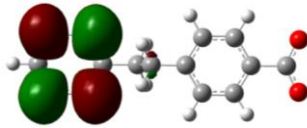
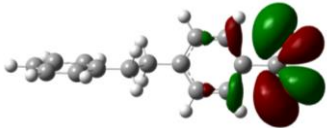
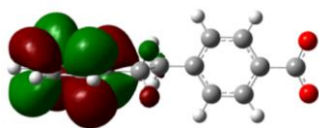
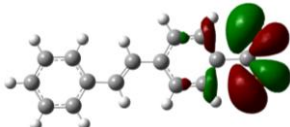
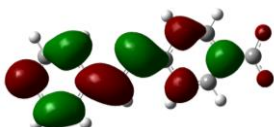
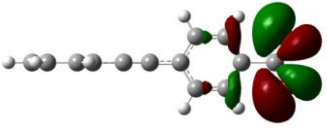
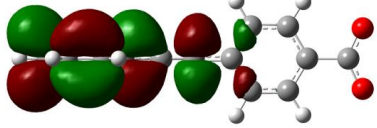


Table S1. Calculated HOMO and LUMO energies of the selected carboxylate anions using density function theory (DFT B3LYP/6-31G+(d, p)).

Molecule	HOMO (eV)	LUMO (eV)
[O₂C(C₆H₄)₂H][−] *The dihedral angle of two phenylene rings is 37.26 degrees.	 -1.708	 1.461
[O₂C(C₆H₄)(CH₂–CH₂)(C₆H₄)H][−] *Two phenylene rings are coplanar.	 -1.674	 1.269
[O₂C(C₆H₄)(CH=CH)(C₆H₄)H][−] *Two phenylene rings are perpendicular.	 -1.672	 1.250
[O₂C(C₆H₄)(C≡C)(C₆H₄)H][−] *Two phenylene rings are coplanar.	 -1.902	 0.608
[O₂C(C₆H₄)(C≡C)(C₆H₄)H][−] *Two phenylene rings are perpendicular.	 -1.951	 0.697

Transmission Theory for Molecular Series Junctions

In a MMM junction, charge crosses a tunneling barrier whose energetic topography is not exactly known, but is determined by the insulating molecular component (e.g., the SAM) between the two metallic contacts. In principle, one approach to measuring the relative height of the tunneling barrier in a MMM junction is to study β systematically for each functional group that influences the barrier topography (and thus the rate or mechanism of charge transport) and to use these values to estimate energetic topography of the HOMO.

Here, we derive the rules for a molecular series circuit using two different approaches: 1) a potential barrier model along with the wavefunction method; 2) a tight-binding model together with the Green's function method.

Modeling of Experimental Setup. In order to model the $\text{Ag}^{\text{TS}}/\text{molecule}/\text{Ga}_2\text{O}_3/\text{EGaIn}$ junction, we assume that each part of the junction, i.e., Ag^{TS} , the molecule, $\text{Ga}_2\text{O}_3/\text{EGaIn}$, is isolated, but we regard the combination of the molecule and its interfaces as a whole (corresponding to R_2). Thus, the experimental setup can be expressed as three individual resistors connected in series (Figure S5).

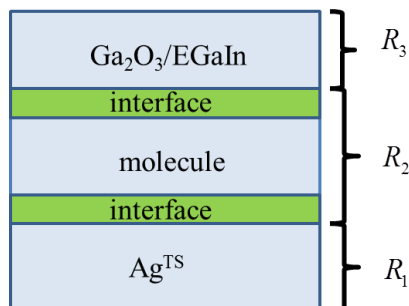
From a macroscopic perspective, the three parts connected in series have an overall resistance of $R_1 + R_2 + R_3$, and the current flux J is equal to the current I divided by the area A (eq. S1),

$$J = \frac{I}{A} = \frac{V_{SD}}{(R_1 + R_2 + R_3)A} \quad \text{Eq. (S1)}$$

and can reduce to the form in eq. S2, since the molecule is considered as an insulating layer which resistance is much larger than that of the electrodes (i.e., $R_2 \gg R_1, R_3$).

$$J \cong \frac{V_{SD}}{R_2 A} \quad \text{Eq. (S2)}$$

Figure S5. The whole system is divided into three parts: bottom electrode, molecule (including its interfaces with the electrodes), and top electrode. Note that the molecules consist of two molecular backbone units: units *a* and *b* (not shown).



Note that the length of the molecule and its interfaces is approximately a few nanometers, so that R_2 (Figure S6) should be modeled using quantum mechanics.

Quantum Tunneling and Landauer Formula. Many reports of electron transport at the single-molecule level ($< 3\sim 4$ nm)²¹⁻²⁵ have shown that the mechanism of charge transport is based on quantum tunneling. At a low bias limit, the conductance g is proportional to the transmission function $T(E_F)$ (eq. S3),²⁶⁻³⁰

$$g \approx \frac{2e^2}{h} T(E_F) = g_Q T(E_F), \quad \text{Eq. (S3)}$$

where h is Planck's constant, e is the elementary charge, g_Q is the so-called conductance quantum, and E_F is the Fermi level of the electrodes. As a result, for a single molecule, we define current as

$$I' \approx \frac{V_{SD}}{R_2} = gV = \frac{2e^2 V_{SD}}{h} T(E_F). \quad \text{Eq. (S4)}$$

For an assembly of molecules in the form of a SAM, there are N molecules in an area A ; when we assume that charge carriers travel along chemical bonds and neglect electron transfer laterally between neighboring molecular wires, we obtain the following equation

$$J = \frac{I}{A} = \frac{\sum_{m=1}^N I'_m}{A} = \frac{1}{A} \frac{2e^2 V_{SD}}{h} \sum_{m=1}^N T_m(E_F), \quad \text{Eq. (S5)}$$

where the index m stands for the m -th molecule. For simplicity, we assume all molecules are identical (the variation in the contacts with the metal electrode can be eliminated because it is an average effect), *i.e.*, $I'_m = I'$ and $T_m(E_F) = T(E_F)$, so we can derive

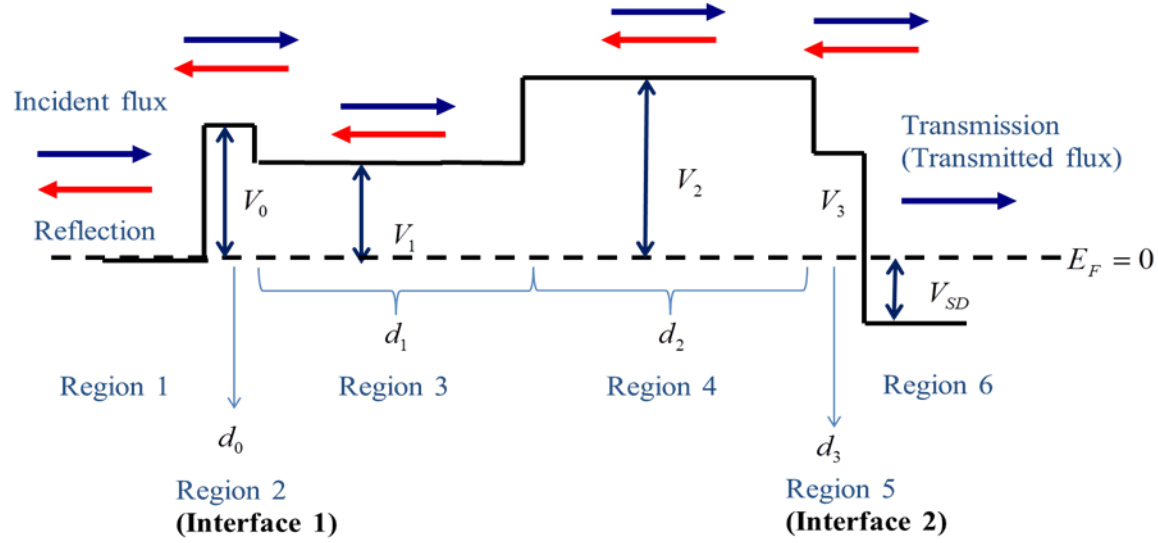
$$J = \frac{N}{A} \frac{2e^2 V_{SD}}{h} T(E_F). \quad \text{Eq. (S6)}$$

Eq. S6 indicates that the key issue of computing J is how to derive the transmission function $T(E_F)$.

Method I: A Potential Barrier Model along with the Wavefunction Method

To model electron transport through the SAM and compute the transmission functions, first, we considered a potential barrier model. The validity of the potential barrier model is based on two assumptions. i.) The tunneling electron does not interact with other degrees of freedom in the molecules, such as phonons (i.e., we assumed coherent elastic tunneling, where “coherent” means no phase loss and “elastic” means no energy loss of electrons). Note that this assumption works well only for short molecules having a large gap between the HOMO (LUMO) and the Fermi level of the electrodes. ii) The electrons in molecules do not interact with each other (an independent electron approximation). Applying this assumption reduces the many-electron Schrodinger equation to an effective single-electron Schrodinger equation, and electrons and nuclei in the SAM can be modeled as potential barriers. Based on these assumptions, the central part can be modeled as shown in Figure S6.

Figure S6. A multi-barrier model. Region 1 (6), 2 (5), and 3(4) correspond to the electrode, interface, and the unit of SAM in Fig 1. d_0 , d_1 , d_2 , and d_3 are the length of the interface 1, unit a , unit b , and interface 2. V_0 , V_1 , V_2 , and V_3 stand for the potential barriers of the interface 1, unit a , unit b , and interface 2. V_{SD} is the source-drain voltage. Blue and red arrows indicate the forward and backward fluxes of a tunneling charge carrier. The two-way arrows (blue and red) represent the incident flux and the one-way arrow (blue) represents the transmitted flux.



According to Figure S6 and the Schrodinger equation $H\psi = E\psi$, where E is the energy of the tunneling electron, we assume the forms of the wavefunction in these five regions are

$$\text{Region 1: } \psi_1 = C_1 \exp(ik_0x) + C_2 \exp(-ik_0x), \text{ where } k_0 = \frac{\sqrt{2mE}}{\hbar} \quad \text{Eq. (S7)}$$

$$\text{Region 2: } \psi_2 = C_3 \exp(ik_1x) + C_4 \exp(-ik_1x), \text{ where } k_1 = \frac{\sqrt{2m(E-V_0)}}{\hbar} \quad \text{Eq. (S8)}$$

$$\text{Region 3: } \psi_3 = C_5 \exp(ik_2x) + C_6 \exp(-ik_2x), \text{ where } k_2 = \frac{\sqrt{2m(E-V_1)}}{\hbar} \quad \text{Eq. (S9)}$$

$$\text{Region 4: } \psi_4 = C_7 \exp(ik_3x) + C_8 \exp(-ik_3x), \text{ where } k_3 = \frac{\sqrt{2m(E-V_2)}}{\hbar} \quad \text{Eq. (S10)}$$

$$\text{Region 5: } \psi_5 = C_9 \exp(ik_4x) + C_{10} \exp(-ik_4x), \text{ where } k_4 = \frac{\sqrt{2m(E-V_3)}}{\hbar} \quad \text{Eq. (S11)}$$

$$\text{Region 6: } \psi_6 = C_{11} \exp(ik_5x), \text{ where } k_5 = \frac{\sqrt{2m(E+V_{SD})}}{\hbar} \quad \text{Eq. (S12)}$$

Using the flux conservation (the continuity of the first derivative of the wavefunction) and the continuity of the wavefunction, solving equations S7 to S12 gives $C_1 \sim C_{11}$.

The transmission function can be expressed in terms of the incident probability current j_{inc} and the transmitted probability current j_{trans} ,²⁸

$$T(E) = \frac{j_{trans}}{j_{inc}}. \quad \text{Eq. (S13)}$$

According to quantum mechanics,²⁸ the probability current j is

$$j = \frac{\hbar}{2mi} (\psi^* \frac{d\psi}{dx} - \frac{d\psi^*}{dx} \psi). \quad \text{Eq. (S14)}$$

Solving equations S7 to S12 using the wavefunction continuity and its first derivative continuity, and substituting eq. S7 and eq. S12 into eq. S14 give j_{inc} and j_{trans} . Moreover, substituting j_{inc} and j_{trans} into eq. S13 provides the transmission function.

Following calculation, we can derive a closed form of the transmission function. Here, we employ the last assumption: the energy of charge carriers is much smaller than the height of potential barrier ($E = E_F \approx 0$); that is, if k_1 , k_2 , k_3 , and k_4 in equations S8 to S11 can satisfy $2k_m d_m \gg 1$, where $m = 1, 2, 3$ and 4 , we can approximate the transmission function as following,

$$T(E_F) = \frac{2^{10} \times V_1 V_2 V_3 V_{SD}}{(\sqrt{V_0} + \sqrt{V_1})^2 (\sqrt{V_1} + \sqrt{V_2})^2 (\sqrt{V_2} + \sqrt{V_3})^2 (V_3 + V_{SD})} \exp(-\phi) \exp(-\beta_1 d_1 - \beta_2 d_2). \quad \text{Eq. (S15)}$$

where ϕ , β_1 , and β_2 can be expressed as follows

$$\phi = \frac{2\sqrt{2mV_0}}{\hbar} d_0 + \frac{2\sqrt{2mV_3}}{\hbar} d_3, \quad \text{Eq. (S16)}$$

$$\beta_1 = \frac{2\sqrt{2mV_1}}{\hbar}, \quad \text{Eq. (S17)}$$

$$\beta_2 = \frac{2\sqrt{2mV_2}}{\hbar}, \quad \text{Eq. (S18)}$$

Substituting equations S15 to S18 into eq. S6, we can derive the current flux. For convenience, we replace the indices 1 and 2 in eq. S19 with the indices a and b in order to represent unit a and b.

$$J = J_0 \exp(-\beta_a d_a - \beta_b d_b), \quad \text{Eq. (S19)}$$

$$J_0 = \frac{N}{A} \frac{2e^2 V_{SD}}{h} \frac{2^{10} \times V_1 V_2 V_3 V_{SD}}{(\sqrt{V_0} + \sqrt{V_1})^2 (\sqrt{V_1} + \sqrt{V_2})^2 (\sqrt{V_2} + \sqrt{V_3})^2 (V_3 + V_{SD})} \exp(-\phi). \quad \text{Eq. (S20)}$$

Note: The calculated values of V , however, are generally overestimated, compared to the experimentally derived values of β . Frisbie et al.³¹ reported that the effective barrier (V) should be described as an integration over many barriers (a result of the mixing of molecular orbitals

and metal electrodes), and as an effective barrier to transport, according to the density of states (DOS) theory.³²

Method II: A Tight-Binding Model along with the Green's Function Method

Compared with method I, method II is more general and allows us to consider coherent inelastic tunneling, many-body interactions, light-driven transport, and the influence of the electrodes by introducing self-energy. Here, we do not consider coherent inelastic tunneling, many-body interactions, and light-driven transport, but instead consider the influence of the electrodes on the circuit rule. Therefore, our goal is to show that eq. S11 can be derived using different approaches and the result is independent from the methodology.

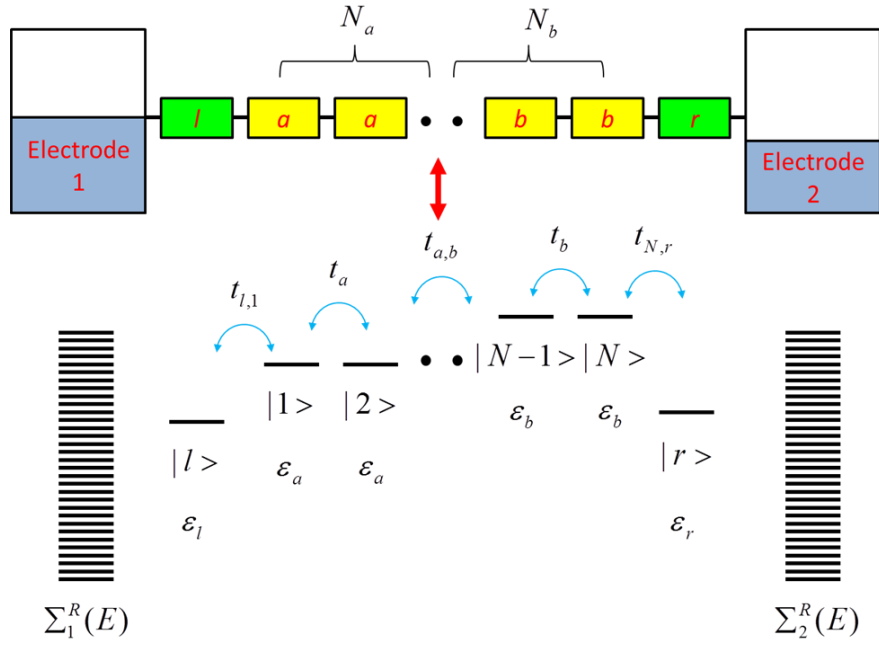
In the framework of the single-particle Green's Function method, the transmission function can be computed using $T(E) = \text{Tr}(\Gamma_1(E)G_{mol}^R(E)\Gamma_2(E)G_{mol}^A(E))$ [6]—[9], where $G_{mol}^{R(A)}(E) = (E - H_{mol} - \Sigma_1^{R(A)}(E) - \Sigma_2^{R(A)}(E))^{-1}$ stands for the retarded (advanced) molecular Green's function and $\Gamma_{1(2)}(E) = i(\Sigma_{1(2)}^R(E) - \Sigma_{1(2)}^A(E))$ represent the coupling function of the electrode 1(2), where $\Sigma_{1(2)}^{R(A)}(E)$ are the retarded (advanced) self-energy contributed from the electrode 1(2).

To facilitate the analysis, we adopted a tight-binding model to describe the SAM. The SAM based on two different molecular backbone units a and b , *e.g.*, a alkyl chain and a phenyl chain, is modeled as shown in Figure S7. The molecular Hamiltonian can be described by eq. S21,

$$\begin{aligned}
 H_{mol} = & \sum_{n_a=1}^{N_a} \epsilon_a |n_a\rangle\langle n_a| + \sum_{n_a=1}^{N_a-1} t_a (|n_a\rangle\langle n_a+1| + |n_a+1\rangle\langle n_a|) \\
 & + \sum_{n_b=N_a+1}^{N_a+N_b} \epsilon_b |n_b\rangle\langle n_b| + \sum_{n_b=N_a+1}^{N_a+N_b-1} t_b (|n_b\rangle\langle n_b+1| + |n_b+1\rangle\langle n_b|) \\
 & + t_{a,b} (|N_a\rangle\langle N_a+1| + |N_a+1\rangle\langle N_a|) + \epsilon_l |l\rangle\langle l| + \epsilon_r |r\rangle\langle r| \\
 & + t_{l,1} (|1\rangle\langle 1| + |1\rangle\langle l|) + t_{N,r} (|r\rangle\langle N| + |N\rangle\langle r|),
 \end{aligned} \tag{S21}$$

where $\epsilon_{l(r)}$ is the on-site energy of the left (right) anchor group, $\epsilon_{a(b)}$ stands for the on-site energy on the unit of the backbone $a(b)$ which has the number of units N_a (N_b). The total number of sites is $N = N_a + N_b$, $t_{a(b)}$ is the resonance integral between the sites on the backbone $a(b)$, $t_{a,b}$ is the resonance integral between the sites on the backbone a and b , and $t_{m,m'}$ is the resonance integral between the site m and m' (Note that $m(m') = 1, N, l, r$).

Figure S7. A tight-binding model of the central part.



Because the molecular backbone units are not directly coupled to electrodes 1 and 2, we assume that the self-energy, contributed by the electrodes, only interacts with the anchor groups (i.e.,

$$\Sigma^{R(A)}(E) = \Sigma_1^{R(A)}(E) + \Sigma_2^{R(A)}(E) = |l\rangle (\Sigma_1^{R(A)}(E))_{l,l} \langle l| + |r\rangle (\Sigma_2^{R(A)}(E))_{r,r} \langle r|. \quad \text{Eq. (S22)}$$

$$(\Sigma_{1(2)}^{R(A)}(E))_{l,l(r,r)} = (\Delta_{1(2)}(E))_{l,l(r,r)} - \frac{i}{2} (\Gamma_{1(2)}(E))_{l,l(r,r)}, \quad \text{Eq. (S23)}$$

$\Delta_{1(2)}(E)$ is the real part of the self-energy of electrode 1 (2), which corresponds to an energy shift resulting from the electrodes; $\Gamma_{1(2)}(E)$ is the imaginary part of the self-energy of electrode 1 (2), which is related to a tunneling rate between electrode 1 (2) and the left (right) anchoring group). At a low bias limit, the self-energy can be regarded as a constant, i.e., $\Delta_{1(2)}(E) = \Delta_{1(2)}$, $\Gamma_{1(2)}(E) = \Gamma_{1(2)}$, and $\Sigma_{1(2)}^R(E) = \Sigma_{1(2)}^R$. By using equations S12 and S13, the retarded molecular Green's function can be represented in a matrix form,

$$G_{\text{mol}}^R = (E_F - H_{\text{mol}} - \Sigma_k^R)^{-1} = \begin{pmatrix} E_F - \epsilon_l - (\Sigma_1^R)_{l,l} & t_{l,a} & 0 & 0 & 0 & 0 & 0 & 0 \\ t_{l,1} & E_F - \epsilon_a & t_a & 0 & 0 & 0 & 0 & 0 \\ 0 & t_a & \ddots & \ddots & 0 & 0 & 0 & 0 \\ 0 & 0 & \ddots & E_F - \epsilon_a & t_{a,b} & 0 & 0 & 0 \\ 0 & 0 & 0 & t_{a,b} & E_F - \epsilon_b & \ddots & 0 & 0 \\ 0 & 0 & 0 & 0 & \ddots & \ddots & t_b & 0 \\ 0 & 0 & 0 & 0 & 0 & t_b & E_F - \epsilon_b & t_{N,r} \\ 0 & 0 & 0 & 0 & 0 & 0 & t_{N,r} & E_F - \epsilon_r - (\Sigma_2^R)_{r,r} \end{pmatrix}.$$

In a weak coupling and large gap limit, i.e., $\min |E - \epsilon_m - \Sigma_{1(2)}^R| \gg \max |t_{m,m'}|$, $(G_{\text{mol}}^R)_{L,R}$ can be approximated as

$$(G_{\text{mol}}^R)_{l,r} = \frac{t_{l,1}}{E_F - \epsilon_l - (\Sigma_1^R)_{l,l}} \cdot \frac{t_{N,R}}{E_F - \epsilon_r - (\Sigma_2^R)_{r,r}} \cdot \frac{t_{a,b}}{t_a t_b} \cdot \left(\frac{t_a}{E_F - \epsilon_a} \right)^{N_a} \left(\frac{t_b}{E_F - \epsilon_b} \right)^{N_b} \quad \text{Eq. (S24)}$$

By using Eq. (24), we can derive the transmission function

$$\begin{aligned}
T(E_F) &= \text{Tr}(\Gamma_1 G_{mol}^R \Gamma_2 G_{mol}^A) \\
&= (\Gamma_1)_{l,l} (\Gamma_2)_{r,r} | (G_{mol}^R)_{l,r} |^2 \\
&= \frac{(\Gamma_1)_{l,l} |t_{l,l}|^2}{|E_F - \varepsilon_L - (\Sigma_1^R)_{l,l}|^2} \cdot \frac{(\Gamma_2)_{r,r} |t_{N,R}|^2}{|E_F - \varepsilon_R - (\Sigma_2^R)_{r,r}|^2} \cdot \frac{|t_{a,b}|^2}{|t_a|^2 |t_b|^2} \cdot \left| \frac{t_a}{E_F - \varepsilon_a} \right|^{2N_a} \left| \frac{t_b}{E_F - \varepsilon_b} \right|^{2N_b}
\end{aligned} \tag{S25}$$

Substituting eq. S25 into eq. S6, we can derive the current flux through the total system

$$J = \frac{N}{A} \frac{2e^2 V_{SD}}{h} \frac{(\Gamma_1)_{l,l} |t_{l,l}|^2}{|E_F - \varepsilon_L - (\Sigma_1^R)_{l,l}|^2} \cdot \frac{(\Gamma_2)_{r,r} |t_{N,R}|^2}{|E_F - \varepsilon_R - (\Sigma_2^R)_{r,r}|^2} \cdot \frac{|t_{a,b}|^2}{|t_a|^2 |t_b|^2} \cdot \left| \frac{t_a}{E_F - \varepsilon_a} \right|^{2N_a} \left| \frac{t_b}{E_F - \varepsilon_b} \right|^{2N_b} \tag{S26}$$

In fact, eq. S26 can correspond to eq. S18. We rewrite eq. S26 as follows

$$J = J_0 \exp(-\beta_a d_a - \beta_b d_b) \tag{S19}$$

$$J_0 = \frac{N}{A} \frac{2e^2 V_{SD}}{h} \frac{(\Gamma_1)_{l,l} |t_{l,l}|^2}{|E_F - \varepsilon_L - (\Sigma_1^R)_{l,l}|^2} \cdot \frac{(\Gamma_2)_{r,r} |t_{N,R}|^2}{|E_F - \varepsilon_R - (\Sigma_2^R)_{r,r}|^2} \cdot \frac{|t_{a,b}|^2}{|t_a|^2 |t_b|^2} \tag{S27}$$

$$\beta_a = \frac{2N_a}{d_a} \ln \left| \frac{E_F - \varepsilon_a}{t_a} \right| \tag{S28}$$

$$\beta_b = \frac{2N_b}{d_b} \ln \left| \frac{E_F - \varepsilon_b}{t_b} \right| \tag{S29}$$

Method II implies that eq. S19 is insensitive to the electrodes in the weak coupling and large gap limit. The weak coupling means that the resonance integral between monomers (units) is weak and the large gap means that the energy level on each monomer (unit) is far away from the Fermi level. Note that the conditions of these two approximations (methods I and II) seem different, but they conclude similarly. For example, the conditions of method I do not specify the extent of electronic couplings between the units in the molecule. However, the assumption that the potential barriers of the two molecular units are independent to the identity of the neighboring units defines a weak electronic coupling between the units. Note that in the experiment results,

(S19) does not hold in serial molecular segments which have strong interactions, consistent with the assumption of the two approaches. In addition, method I cannot include the effects of electrodes while the method II can. The method II successfully explains that the influence of the electrodes.

By using the definition of resistance, S26, and S27, and (for simplicity) assuming that $N_a = N_b = 1$, we can derive

$$R = \frac{V_{SD}}{JA} = \frac{V_{SD}}{J_0 A} \left| \frac{E_F - \epsilon_a}{t_a} \right|^2 \left| \frac{E_F - \epsilon_b}{t_b} \right|^2 \quad \text{Eq. (S 30)}$$

The resistance of a molecular segment can be defined as³³ $R_a = R_Q \left| \frac{E_F - \epsilon_a}{t_a} \right|^2$ and $R_b = R_Q \left| \frac{E_F - \epsilon_b}{t_b} \right|^2$,

S 30 becomes

$$R = \frac{V_{SD}}{J_0 A} \frac{R_a}{R_Q} \times \frac{R_b}{R_Q} \propto \frac{R_a}{R_Q} \times \frac{R_b}{R_Q} \propto R_a \times R_b \quad \text{Eq. (S 31)}$$

Where $R_Q = g_Q^{-1}$. S31 is consistent with the results reported in previous studies,³⁴⁻³⁶ that in a quantum tunneling, the total resistance of a molecular junction is proportional to the product of the individual molecular units.

References

- (1) Salomon, A.; Cahen, D.; Lindsay, S.; Tomfohr, J.; Engelkes, V. B.; Frisbie, C. D. *Adv. Mater.* **2003**, *15*, 1881.
- (2) Tran, E.; Grave, C.; Whitesides, G. M.; Rampi, M. A. *Electrochim. Acta* **2005**, *50*, 4850.
- (3) Tao, N. J. *Nat. Nanotechnol.* **2006**, *1*, 173.
- (4) Aradhya, S. V.; Venkataraman, L. *Nat. Nanotechnol.* **2013**, *8*, 399.
- (5) Schlotter, N. E.; Porter, M. D.; Bright, T. B.; Allara, D. L. *Chem. Phys. Lett.* **1986**, *132*, 93.
- (6) Allara, D. L.; Nuzzo, R. G. *Langmuir* **1985**, *1*, 52.
- (7) Allara, D. L.; Nuzzo, R. G. *Langmuir* **1985**, *1*, 45.
- (8) Tao, Y. T. *J. Am. Chem. Soc.* **1993**, *115*, 4350.
- (9) Tao, Y. T.; Lee, M. T.; Chang, S. C. *J. Am. Chem. Soc.* **1993**, *115*, 9547.
- (10) Liao, K.-C.; Yoon, H. J.; Bowers, C. M.; Simeone, F. C.; Whitesides, G. M. *Angew. Chem. Int. Ed.* **2014**, *53*, 3889.
- (11) Weiss, E. A.; Kaufman, G. K.; Kriebel, J. K.; Li, Z.; Schalek, R.; Whitesides, G. M. *Langmuir* **2007**, *23*, 9686.
- (12) Bowers, C. M.; Liao, K.-C.; Yoon, H. J.; Rappoport, D.; Baghbanzadeh, M.; Simeone, F. C.; Whitesides, G. M. *Nano Lett.* **2014**, *14*, 3521.
- (13) Cademartiri, L.; Thuo, M. M.; Nijhuis, C. A.; Reus, W. F.; Tricard, S.; Barber, J. R.; Sodhi, R. N. S.; Brodersen, P.; Kim, C.; Chiechi, R. C.; Whitesides, G. M. *J. Phys. Chem. C* **2012**, *116*, 10848.
- (14) Chiechi, R. C.; Weiss, E. A.; Dickey, M. D.; Whitesides, G. M. *Angew. Chem. Int. Ed.* **2008**, *47*, 142.
- (15) Nijhuis, C. A.; Reus, W. F.; Barber, J. R.; Whitesides, G. M. *J. Phys. Chem. C* **2012**, *116*, 14139.
- (16) Simeone, F. C.; Yoon, H. J.; Thuo, M. M.; Barber, J. R.; Smith, B.; Whitesides, G. M. *J. Am. Chem. Soc.* **2013**, *135*, 18131.
- (17) Yuan, L.; Jiang, L.; Thompson, D.; Nijhuis, C. A. *J. Am. Chem. Soc.* **2014**.
- (18) Yoon, H. J.; Shapiro, N. D.; Park, K. M.; Thuo, M. M.; Soh, S.; Whitesides, G. M. *Angew. Chem. Int. Ed.* **2012**, *51*, 4658.

- (19) Reus, W. F.; Nijhuis, C. A.; Barber, J. R.; Thuo, M. M.; Tricard, S.; Whitesides, G. M. *J. Phys. Chem. C* **2012**, *116*, 6714.
- (20) Liao, K. C.; Bowers, C. M.; Yoon, H. J.; Whitesides, G. M. *J. Am. Chem. Soc.* **2015**, *137*, 3852.
- (21) Ho Choi, S.; Kim, B.; Frisbie, C. D. *Science* **2008**, *320*, 1482.
- (22) Lu, Q.; Liu, K.; Zhang, H.; Du, Z.; Wang, X.; Wang, F. *ACS Nano* **2009**, *3*, 3861.
- (23) Choi, S. H.; Risko, C.; Delgado, M. C. R.; Kim, B.; Brédas, J.-L.; Frisbie, C. D. *J. Am. Chem. Soc.* **2010**, *132*, 4358.
- (24) Sedghi, G.; Garcia-Suarez, V. M.; Esdaile, L. J.; Anderson, H. L.; Lambert, C. J.; Martin, S.; Bethell, D.; Higgins, S. J.; Elliott, M.; Bennett, N.; Macdonald, J. E.; Nichols, R. J. *Nat. Nanotech.* **2011**, *6*, 517.
- (25) Zhao, X.; Huang, C.; Gulcur, M.; Batsanov, A. S.; Baghernejad, M.; Hong, W.; Bryce, M. R.; Wandlowski, T. *Chem. Mater.* **2013**, *25*, 4340.
- (26) Datta, S. *Quantum Transport : Atom to Transistor* **2005**.
- (27) Di Ventra, M. *Electrical Transport in Nanoscale Systems* **2008**.
- (28) Davies, J. H. *Physics of Low-Dimensional Semiconductors* **1998**.
- (29) Hsu, L.-Y.; Li, E. Y.; Rabitz, H. *Nano Lett.* **2013**, *13*, 5020.
- (30) Hsu, L.-Y.; Huang, Q.-R.; Jin, B.-Y. *J. Phys. Chem. C* **2008**, *112*, 10538.
- (31) Engelkes, V. B.; Beebe, J. M.; Frisbie, C. D. *J. Am. Chem. Soc.* **2004**, *126*, 14287.
- (32) Xue, Y.; Datta, S.; Ratner, M. A. *J. Chem. Phys.* **2001**, *115*, 4292.
- (33) Huang, M.-J.; Hsu, L.-Y.; Fu, M.-D.; Chuang, S.-T.; Tien, F.-W.; Chen, C.-h. *J. Am. Chem. Soc.* **2014**, *136*, 1832.
- (34) Joachim, C.; Gimzewski, J. K.; Aviram, A. *Nature* **2000**, *408*, 541.
- (35) Joachim, C.; Ratner, M. A. *Proc. Natl. Acad. Sci. USA* **2005**, *102*, 8801.
- (36) Joachim, C. *Nat. Nanotech.* **2012**, *7*, 620.